AIAA JOURNAL
Vol. 30, No. 12, December 1992

Structural Behavior of Two-Cell Composite Rotor Blades with Elastic Couplings

Ramesh Chandra* and Inderjit Chopra†
University of Maryland, College Park, Maryland 20742

This paper presents an analytical-cum-experimental study of the structural response of composite rotor blades with elastic couplings. Vlasov theory is expanded to analyze two-cell composite rotor blades made out of general composite laminates including the transverse shear deformation of the cross section. Variation of shear stiffness along the contour of the section is included in the warping function. To validate this analysis, two-cell graphite-epoxy composite blades with extension-torsion coupling were fabricated using a matched-die molding technique. These blades were tested under tip bending and torsional loads, and their structural response in terms of bending slope and twist was measured with a laser optical system. Good correlation between theory and experiment was achieved. Axial force-induced twist rate of the order of 10 deg per meter length (0.25 deg per inch length) due to a 4.45-kN (1000-lb) force can be realized in extension-torsion coupled blades with a hygrothermally stable lay-up $[20/-70]_{2s}$ for potential applications in the design of tilt rotors.

Nomenclature

c, t	= chord and thickness of blade
E_l, E_t	= Young's moduli of plies in principal directions
F	= axial force at the tip of blade
G_{lt}	= shear modulus of plies in principal plane
K_{ij}	= stiffness matrix for blade
k_s, k_z, k_{sz}	= bending curvatures referring to plate segment of blade
l	= length of blade
M_s, M_z, M_{sz}	= moment resultants referring to plate segment of blade
M_x, M_y	= bending moments referring to blade
M_ω	= bimoment (or warping moment) referring to blade
N	= axial force referring to blade
N_s, N_z, N_{sz}	= stress resultants referring to plate segment of blade
n, s, z	= coordinate system for plate segment of blade
P	= applied force at tip of blade
T	= torsion moment referring to blade
$\bar{T}$	= applied torsion at tip of blade
U, V, W	= displacements in x, y, z directions, respectively, referring to blade
u, v, w	= displacements in n, s, z directions, respectively, referring to plate segment of blade
V_x, V_y	= shear forces in x and y directions, respectively, referring to blade
x, y, z	= coordinate system for blade
ϵ_s, ϵ_z, ϵ_{sz}	= membrane strains referring to plate segment of blade
ϵ_{xz}, ϵ_{yz}	= transverse shear strains for the blade in xz and yz planes, respectively
μ	= constrained warping parameter
μ_{lt}	= Poisson's ratio of plies in principal plane
σ_s, σ_z, σ_{sz}	= stress field referring to plate segment of blade
ϕ_x, ϕ_y, ϕ_z	= rotations about x, y, z axes, respectively, referring to blade
φ	= warping function

Superscripts

skb	= bottom part of skin of blade
skt	= top part of skin of blade
spb	= bottom part of spar of blade
spt	= top part of spar of blade
w	= web of blade
$'$	= differentiation with respect to z coordinate of blade

Introduction

WITH the application of high-performance composite materials, the design feasibility of advanced rotor systems such as hingeless and bearingless rotors is becoming a reality. Superior fatigue characteristics and flexibility to tailor structural characteristics are the key factors for the growing application of composites in the rotorcraft industry. Because of the nonavailability of validated composite analytical models, an extreme level of conservatism is used in rotorcraft design, and the potential benefits of structural couplings due to composites are not exploited at this time. Analyses of composite blade structures are more involved because nonclassical phenomena such as section warping and transverse shear related coupling become significant. For the full exploration of composites to improve the performance of current helicopters and also to meet many challenging missions of future helicopters, it is necessary to develop and validate analyses of composite blades with elastic couplings.

Helicopter rotor blades are slender and are normally modeled as elastic beams. Research studies on the modeling of coupled composite beams can be classified into four categories: solid rectangular cross section, open section, single-cell closed section, and multicell airfoil section.

References 1-3 investigated solid cross-section composite beams. Johnson[1] presented bending-torsion behavior of anisotropic beams in the small deflection regime under static loads. In that investigation, a variational method was used to predict the effective bending stiffness of bending-torsion coupled beams. Minguet and Dugundji[2,3] presented an analytical-experimental study of composite beams in the large deflection regime under static and dynamic loading conditions. The large deflection analysis used Euler angles to include arbitrarily large deformation without the need for an ordering scheme. For their dynamic analysis, small-amplitude vibrations about the static deflected position of the beam were calculated using an influence coefficient method together with a finite differ-

Received Nov. 25, 1991; revision received April 26, 1992; accepted for publication May 1, 1992.

*Assistant Research Scientist, Department of Aerospace Engineering. Member AIAA.

†Professor, Department of Aerospace Engineering. Fellow AIAA.

ence solution. Calculated results were correlated satisfactorily with measured values for several composite coupled beams.

Under the category of open-section composite beams, Chandra and Chopra[4,5] presented a theoretical-cum-experimental study on static and dynamic behavior of composite I-beams. Such open-section composite beams are routinely used in the construction of flex beams of a bearingless rotor. Their analysis was based on Vlasov theory[6,7] for beams made out of general composite laminates, including transverse shear deformation. The Galerkin method was used to predict free vibration characteristics of coupled composite I-beams under rotation. Graphite-epoxy and Kevlar-epoxy beams were built and tested for static and vibration characteristics. An in-vacuo rotor test facility was used to provide rotating vibration data for correlation to the analytical predictions. Modeling of constrained warping effects and general layered composite lamination of the walls of composite open-section beams was considered mandatory to predict their structural response. Rehfield and Atilgan[8] presented a buckling analysis of composite open-section beams. They included transverse shear deformation, but neglected the bending stiffness of the wall.

Hong and Chopra[9] studied the aeroelastic stability of hingeless rotor blades where the blade was modeled as a single-cell, thin-wall, rectangular section composite beam. That investigation showed a significant influence of elastic couplings caused by layered composites on blade dynamics. Chandra et al.[10] evaluated the composite structural model of Ref. 9 by finite element and experimental techniques for bending-torsion and extension-torsion coupled composite box beams. The poor correlation was attributed to inadequate modeling of nonclassical effects. Smith and Chopra[11] introduced transverse shear effects into the structural model of Ref. 9. Also, the variation of shear stiffness along the contour of the section was incorporated in the warping function. These refinements helped improve the correlation of predicted static response results with measured values. Chandra and Chopra[12] presented theoretical and experimental vibration characteristics of composite box beams under rotation. In that study, the analysis was based on the structural model of Ref. 11, and the Galerkin method was used to predict natural frequencies and mode shapes of composite box beams with couplings. Predicted frequencies and mode shapes correlated satisfactorily with measured values for several composite box beams.

Rehfield et al.[13] presented a beam theory for composite single-cell box beams with extension-twist couplings. The analytical model used contour analysis and neglected the local bending stiffness of the thin-walled beams. Experimental correlation was provided for extension-torsion coupled beams. That study showed the importance of transverse shear deformation for composite box beam analysis. Hodges et al.[14] presented a theoretical study on free-vibration characteristics of composite beams without rotation. The analysis was based on the structural model of Ref. 13. The equations of motion were solved by exact integration and mixed finite element methods. Rehfield et al.[15] extended their earlier structural modeling to multicell composite beams.

Kosmatka[16] used an elasticity approach to investigate the influence of initial twist on the structural behavior of composite beams. Single-cell D section beams with initial twist were analyzed. The importance of initial twist in the modeling of rotor blades was highlighted. Bauchau and Hong[17] presented a large deflection finite element analysis of curved and twisted composite beams. The analysis that included transverse shear and torsion related warping was correlated by experiments. Giavotto et al.[18] presented a finite element analysis for anisotropic beams. Borri and Merlini[19] formulated a composite beam theory from a virtual work approach, where large rotations and accurate cross-section warping were included. Nixon[20] examined the elastic twist requirements for full-scale extension-twist coupled tilt-rotor blades. He used the beam theory of Ref. 13 to predict the elastic twist of circular composite tubes representative of tilt-rotor blades under torsion and axial loads. The potential of elastic couplings due to composites was shown to improve tilt-rotor performance.

The previously mentioned studies show that the important nonclassical effects in the analysis of thin-walled composite beams are cross-section warping and transverse shear related elastic couplings. Most analyses are confined to single-cell, thin-walled, box beams. The objective of the present investigation is to formulate a structural analysis of a two-cell composite rotor blade in the regime of small deflection theory including these nonclassical effects and then to validate the analysis by experiments.

Analysis

In this paper, Vlasov theory is expanded to analyze a two-cell spar-skin rotor blade made out of general composite laminates. Transverse shear effects are included. The essence of this theory is the reduction of two-dimensional stress and displacement fields (associated with plate/shell segments of the blade) to one-dimensional stresses and displacements identified with the blade as a beam. The six generalized blade displacements are determined from the plate/shell displacements through geometric considerations; whereas, the generalized blade forces and their equilibrium equations are obtained by invoking the principle of virtual work.

The present analysis uses three coordinate systems: an orthogonal right-handed Cartesian coordinate system (x, y, z) for the blade; an orthogonal coordinate system (n, s, z) for any plate segment of the blade where the n axis is normal to the midsurface of any plate segment, the s axis is tangential to the midsurface and is along the contour line of the blade cross section, and the z axis is along the longitudinal axis of blade, Fig. 1a; and a contour coordinate system s, where s is measured along the contour line of the cross section from a judiciously selected origin, Fig. 1b. The seven generalized blade forces are V_x, V_y, V_z, M_x, M_y, T, and M_ω. The torsional moment T consists of unconstrained warping torsion (Saint Venant torsion) and constrained warping torsion (Vlasov torsion). As shown later, the Vlasov torsion and bimoment M_ω are related to each other.

Fundamental Assumptions

Three basic assumptions used in the present theory are the following:

1) The contour (midline of the plate segments) of a cross section does not deform in its plane. This means that the in-plane warping of the cross section is neglected and the normal strain ϵ_s in the contour direction is neglected in comparison with the normal axial strain ϵ_z. This assumption was introduced by Vlasov.[6]

2) The normal stress σ_s is neglected in comparison with axial stress σ_z.

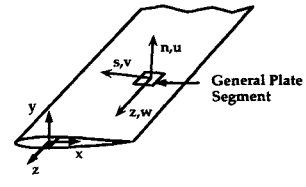

Fig. 1a Cartesian coordinates in rotor blade.

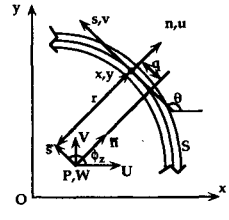

Fig. 1b Pictorial definitions of blade displacements and rotations.

3) Any general plate segment of the blade is governed by linear classical laminated plate theory. This implies that the transverse shear deformation of the plate segment is not accounted for, though the transverse shear deformation of the blade is considered.

These assumptions imply that the nonzero membrane strains and bending curvatures for the plate segment are ϵ_z, ϵ_{sz}, k_z, and k_{sz}.

Kinematics

In the present formulation, each blade segment is idealized as a thin laminated composite plate. From geometric considerations Fig. 1b, the plate displacements $u(s, z)$ and $v(s, z)$ are related to the blade displacements U, V and ϕ_z as

$$u(s, z) = U(z) \sin \theta(s) - V(z) \cos \theta(s) - q(s)\phi_z(z) \quad (1)$$

$$v(s, z) = U(z) \cos \theta(s) + V(z) \sin \theta(s) + r(s)\phi_z(z) \quad (2)$$

where r, q, and θ are shown in Fig. 1b. We obtain $w(s, z)$ using the following shear strain-displacement relation:

$$\epsilon_{sz} = w_{,s} + v_{,z} \quad (3)$$

The shear strain ϵ_{sz} consists of two components: one due to transverse shear effects and the other due to torsion. Hence, ϵ_{sz} is given by

$$\epsilon_{sz} = \epsilon_{xz} \cos \theta + \epsilon_{yz} \sin \theta + \epsilon_{sz}^{(s)} \quad (4)$$

It is assumed that shear strain $\epsilon_{sz}^{(s)}$ distribution in the contour direction is similar to the one corresponding to the St. Venant torsion.

From Ref. 7, $\epsilon_{sz}^{(s)}$ is given by

$$\epsilon_{sz}^{(s)}(s, z) = \frac{F(s)}{t(s)} \phi_z'(z) \quad (5)$$

$F(s)$ controls the variation of this shear strain along the contour of the blade cross section. To account for variation of shear modulus G along the contour, Eq. (5) is rewritten as

$$\epsilon_{sz}^{(s)}(s, z) = \frac{G_s(s)}{Gt} \phi_z'(z) \quad (6)$$

where $G_s(s) = F(s)G(s)$. $G_s(s)$ is determined using the compatibility condition for warping deformation.[7] Figure 2 shows a two-cell blade section. It has two circuits for shear flow with five branches. Invoking the condition of net warping deformation over each circuit to be zero, the following equation is obtained

$$\oint_i dw = \oint_i \frac{\partial w}{\partial s} ds = 0, \qquad i = 1, 2 \quad (7)$$

Using Eqs. (2-4) in Eq. (7), the following equations are obtained

$$\oint \frac{G(s)}{Gt} ds = 2A_i \quad (8)$$

where

$$A_i = \oint_i r \, ds$$

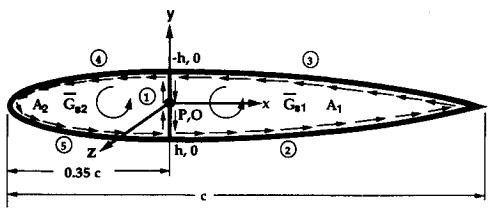

Fig. 2 Schematic of two-cell blade section.

For a single-cell section, G_s is obtained from relation (8) as follows:

$$G_s = 2A \Big/ \left(\oint \frac{1}{Gt} ds \right)$$

Equation (8) is used to compute $G_s(s)$. $\bar{G}_{s1}$ and $\bar{G}_{s2}$ are the values of G_s associated with circuits, and G_{s1} to G_{s5} are the values of G_s associated with branches. From Fig. 2,

$$\begin{aligned} G_{s1} &= \bar{G}_{s1} - \bar{G}_{s2} \\ G_{s2} &= \bar{G}_{s1} \\ G_{s3} &= \bar{G}_{s1} \\ G_{s4} &= \bar{G}_{s2} \\ G_{s5} &= \bar{G}_{s2} \end{aligned} \quad (9)$$

Using relation (8) for two circuits,

$$\bar{G}_{s1}\left[\int_{-h}^{h} \frac{ds_1}{G_1 t_1} + \int_0^{p_1} \frac{ds_2}{G_2 t_2} + \int_0^{p_1} \frac{ds_3}{G_3 t_3} \right] - \bar{G}_{s2} \int_{-h}^{h} \frac{ds_1}{G_1 t_1} ds_1 = 2A_1 \quad (10)$$

$$\bar{G}_{s2}\left[\int_{-h}^{h} \frac{ds_1}{G_1 t_1} + \int_0^{p_2} \frac{ds_4}{G_4 t_4} + \int_0^{p_2} \frac{ds_5}{G_5 t_5} \right] - \bar{G}_{s1} \int_{-h}^{h} \frac{ds_1}{G_1 t_1} ds_1 = 2A_2 \quad (11)$$

where

$$p_1 = \int_{0.35c}^{c} ds, \qquad p_2 = \int_0^{0.35c} ds$$

$$A_1 = 2\int_{0.35c}^{c} y \, dx, \qquad A_2 = 2\int_0^{0.35c} y \, dx$$

Solving Eqs. (10) and (11),

$$\bar{G}_{s1} = \frac{A_1[(h/A_{66}^{(w)}) + (p_2/A_{66}^{(sp)})] + A_2(h/A_{66}^{(w)})}{[(h/A_{66}^{(w)}) + (p_1/A_{66}^{(sk)})][(h/A_{66}^{(w)}) + (p_2/A_{66}^{(sp)})] - (h/A_{66}^{(w)})^2} \quad (12)$$

$$\bar{G}_{s2} = \frac{A_2[(h/A_{66}^{(w)}) + (p_1/A_{66}^{(sk)})] + A_1(h/A_{66}^{(w)})}{[(h/A_{66}^{(w)}) + (p_1/A_{66}^{(sk)})][(h/A_{66}^{(w)}) + (p_2/A_{66}^{(sp)})] - (h/A_{66}^{(w)})^2} \quad (13)$$

Using relations (2-4) and (6), w is obtained as

$$w = W + x\phi_x + y\phi_y - \varphi\phi_z' \quad (14)$$

where the warping function φ is equal to

$$\varphi = \int_0^s \left(r - \frac{G_s}{Gt} \right) ds \quad (15)$$

$$\begin{aligned} \phi_x &= \epsilon_{xz} - U' \\ \phi_y &= \epsilon_{yz} - V' \end{aligned} \quad (16)$$

It is important to note that in Eq. (15) the second term in the parentheses of the integral is zero for an open section. Plate strain ϵ_z is related by the following equation:

$$\epsilon_z = w_{,z} \quad (17)$$

Using relations (14) and (17), ϵ_z is obtained as

$$\epsilon_z = W' + x\phi_x' + y\phi_y' - \varphi\phi_z'' \quad (18)$$

Similarly, k_z and k_{zs} are obtained as

$$k_z = -\sin \theta \phi_x' + \cos \theta \phi_y' - q\phi_z'' + \epsilon_{xz}' \sin \theta - \epsilon_{yz}' \cos \theta \quad (19)$$

$$k_{zs} = -2\phi_z' \tag{20}$$

Thus, the nonzero membrane strains and bending curvatures in the plate segment are given by relations (4) and (18-20).

Plate Stress Field

Using classical laminated plate theory, the stress resultants and moment resultants are

$$\begin{aligned} N_z &= A_{11}\epsilon_z + A_{16}\epsilon_{zs} + B_{11}k_z + B_{16}k_{zs} \\ N_{zs} &= A_{16}\epsilon_z + A_{66}\epsilon_{zs} + B_{16}k_z + B_{66}k_{zs} \\ M_z &= B_{11}\epsilon_z + B_{16}\epsilon_{zs} + D_{11}k_z + D_{16}k_{zs} \\ M_{zs} &= B_{16}\epsilon_z + B_{66}\epsilon_{zs} + D_{16}k_z + D_{66}k_{zs} \end{aligned} \tag{21}$$

Here, the flanges and web of D spar and blade skin are treated as general composite laminates.

Blade Forces and Their Equilibrium Equations

The generalized blade forces and their equilibrium equations are derived by applying the principle of virtual work. Following the procedure used in Ref. 4, the governing equations are obtained as (see Ref. 21) the following:

$$N' + n = 0 \tag{22}$$

$$M_y'' + m_y' - v_x = 0 \tag{23}$$

$$M_x'' + m_x' + v_y = 0 \tag{24}$$

$$M_\omega'' - T_s' + m_\omega' - t' = 0 \tag{25}$$

$$F_x' - G_x + f_x = 0 \tag{26}$$

$$F_y' - G_y + f_y = 0 \tag{27}$$

Blade Force—Displacement Relations

There are nine generalized blade forces, namely, N, M_y, M_x, M_ω, T_s, F_x, F_y, G_x, and G_y, appearing in Eqs. (22-27). These nine generalized forces are related to six generalized displacements. Using plate stress-strain relations [Eq. (21)] and plate strain-beam displacement relations [Eqs. (4) and (18-20)], the relations between the generalized blade forces and displacement are obtained as

$$\begin{bmatrix} N \\ M_x \\ -M_y \\ M_\omega \\ T_s \\ G_x \\ G_y \\ F_x \\ F_y \end{bmatrix} = \begin{bmatrix} K_{11} & K_{12} & K_{13} & K_{14} & K_{15} & K_{16} & K_{17} & K_{18} & K_{19} \\ & K_{22} & K_{23} & K_{24} & K_{25} & K_{26} & K_{27} & K_{28} & K_{29} \\ & & K_{33} & K_{34} & K_{35} & K_{36} & K_{37} & K_{38} & K_{39} \\ & & & K_{44} & K_{45} & K_{46} & K_{47} & K_{48} & K_{49} \\ & & & & K_{55} & K_{56} & K_{57} & K_{58} & K_{59} \\ & & & & & K_{66} & K_{67} & K_{68} & K_{69} \\ & & \text{Symmetric} & & & & K_{77} & K_{78} & K_{79} \\ & & & & & & & K_{88} & K_{89} \\ & & & & & & & & K_{99} \end{bmatrix} \begin{bmatrix} W' \\ \phi_y' \\ \phi_x' \\ \phi_z'' \\ \phi_z' \\ \epsilon_{xz} \\ \epsilon_{yz} \\ \epsilon_{xz}' \\ \epsilon_{yz}' \end{bmatrix} \tag{28}$$

where K_{ij} are given in Ref. 21.

Extension-Torsion Coupled Blades Under Extensional, Torsional, and Bending Loads

Figure 3 shows the lay-up details for extension-torsion coupled blades. Note that the spar has $[0/\theta]$ lay-up, whereas the skin has $[+\theta/-\theta]$ lay-up. The θ layer in the spar causes antisymmetry with respect to the midplane and, hence, creates extension-torsion coupling in the blade. For these blades, simplified force-displacement relations are the following:

Extension-torsion:

$$N = K_{11}W' + K_{15}\phi_z' \tag{29}$$

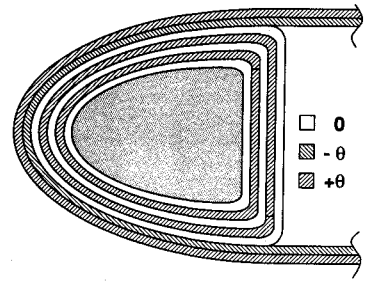

Fig. 3 Lay-up of extension-torsion coupled blades.

$$T_s = K_{15}W' + K_{55}\phi_z' \tag{30}$$

$$M_\omega = K_{44}\phi_z'' \tag{31}$$

Including the influence of constrained warping,[4] the total torsion is given by

$$T = -K_{44}\phi_z'' + K_{15}W' + K_{55}\phi_z' \tag{32}$$

The relations (29) and (32) control the extension-torsion coupled behavior of these blades. These equations are solved for cantilever beams as follows:

Tip torsional load:

$$N = 0; \qquad T = \overline{T} \tag{33}$$

Combining Eqs. (29), (32), and (33)

$$\overline{T} = -K_{44}\phi_z'' + (K_{55})_r\phi_z' \tag{34}$$

where

$$(K_{55})_r = K_{55} - \frac{K_{15}^2}{K_{11}}$$

Equation (34) is solved using the procedure given in Ref. 4 and tip twist is given as

$$\phi_z(z = l) = \frac{\overline{T}l}{(K_{55})_r}\left(1 - \frac{2}{\mu}\tanh\frac{\mu}{2}\right) \tag{35}$$

where

$$\mu = \sqrt{\frac{(K_{55})_r}{K_{44}}}\,l$$

Note that the first term in Eq. (35) refers to St. Venant (free warping) torsion and the second term refers to Vlasov (constrained warping) torsion. Also, the constrained warping parameter μ, which in turn depends on the stiffnesses and length of the blade, controls the significance of constrained warping torsion on twist. For these blades, the constrained warping parameter is higher than 40, hence, the constrained warping effect is highly localized and does not influence their twists.

Axial force:

Similarly induced tip twist in blades under axial force is obtained as

$$\phi_z(z = l) = -\frac{K_{15}}{K_{11}}\frac{Fl}{(K_{55})_r}\left(1 - \frac{2}{\mu}\tanh\frac{\mu}{2}\right) \tag{36}$$

Bending-transverse shear:

$$\begin{Bmatrix} M_x \\ G_x \end{Bmatrix} = \begin{bmatrix} K_{22} & K_{26} \\ K_{26} & K_{66} \end{bmatrix} \begin{Bmatrix} \phi_y' \\ \epsilon_{xz} \end{Bmatrix} \tag{37}$$

$$\begin{Bmatrix} -M_y \\ G_y \end{Bmatrix} = \begin{bmatrix} K_{33} & K_{37} \\ K_{37} & K_{77} \end{bmatrix} \begin{Bmatrix} \phi_x' \\ \epsilon_{yz} \end{Bmatrix} \tag{38}$$

where K_{ij} are given in the Appendix.

Table 1 Details of extension-torsion coupled composite blades

NACA 0012 airfoil	
Material: Graphite-epoxy	
E_l	131 GPa (19×10^6 psi)
E_t	9.3 GPa (1.35×10^6 psi)
G_{lt}	5.86 GPa (0.85×10^6 psi)
μ_{lt}	0.40
Ply thickness	0.127 mm (0.005 in.)
Length	711.2 mm (28 in.)
Chord	76.2 mm (3 in.)
Airfoil thickness	9.144 mm (0.36 in.)

	D spar			
Case	Top flange	Bottom flange	Web	Skin
Blade 1	$[0]_4$	$[0]_4$	$[0]_4$	$[15/-15]$
Blade 2	$[0/15]_2$	$[0/15]_2$	$[0/15]_2$	$[15/-15]$
Blade 3	$[0/30]_2$	$[0/30]_2$	$[0/30]_2$	$[30/-30]$
Blade 4	$[0/45]_2$	$[0/45]_2$	$[0/45]_2$	$[45/-45]$
Blade 5[a]	$[20/-70]_{2s}$	$[20/-70]_{2s}$	$[20/-70]_{2s}$	$[20/-70]$
Blade 6	$[20/-70]_4$	$[20/-70]_4$	$[20/-70]_4$	$[20/-70]$
Blade 7	$[15]_4$	$[15]_4$	$[15]_4$	$[15/-15]$

[a]Hygrothermally stable lay-up.

The relations (37) and (38) control the bending behavior of these blades. Note the existence of bending-shear couplings in these relations.

Tip bending load:

For blades subjected to tip bending load P, the bending slope ϕ_y is obtained from relation (37):

$$\phi_y = \frac{P}{K_{22}[1-(K_{26}^2/K_{22}K_{66})]}\left(\frac{z^2}{2} - lz\right) \tag{39}$$

From Eq. (39), the influence of bending-transverse shear coupling K_{26} is seen to decrease the bending stiffness K_{22}.

To satisfy the strength requirements of the blade, the stresses in its different branches can be computed using the present analysis. Generalized displacements corresponding to extension and twist of an extension-torsion coupled blade under unit axial load are obtained using relations (29) and (30) as

$$w' = \frac{K_{55}}{K_{11}K_{55} - K_{15}^2} \tag{40}$$

$$\phi_z' = -\frac{K_{15}}{K_{11}K_{55} - K_{15}^2} \tag{41}$$

Using relations (40) and (41), strains ϵ_z and ϵ_{sz} are obtained as

$$\epsilon_z = \frac{K_{55}}{K_{11}K_{55} - K_{15}^2} \tag{42}$$

$$\epsilon_{sz}^{(1)} = -\frac{\bar{G}_{s1} - \bar{G}_{s2}}{A_{66}^{(w)}} \frac{K_{15}}{K_{11}K_{55} - K_{15}^2} \tag{43}$$

$$\epsilon_{sz}^{(2)} = -\frac{\bar{G}_{s1}}{A_{66}^{(skb)}} \frac{K_{15}}{K_{11}K_{55} - K_{15}^2} \tag{44}$$

$$\epsilon_{sz}^{(3)} = -\frac{\bar{G}_{s1}}{A_{66}^{(skt)}} \frac{K_{15}}{K_{11}K_{55} - K_{15}^2} \tag{45}$$

$$\epsilon_{sz}^{(4)} = -\frac{\bar{G}_{s2}}{A_{66}^{(spt)}} \frac{K_{15}}{K_{11}K_{55} - K_{15}^2} \tag{46}$$

$$\epsilon_{sz}^{(5)} = -\frac{\bar{G}_{s2}}{A_{66}^{(spb)}} \frac{K_{15}}{K_{11}K_{55} - K_{15}^2} \tag{47}$$

Experiments

To validate the analysis, two-cell composite rotor blades with foam core were fabricated using a matched-die molding technique. There are three important aspects of this process: making of rigid foam core, making of foam filled spar, and making of spar-skin-foam rotor blade. The foam core in the required airfoil shape is built using compression molding technique. In this method, rough-machined blank foam is placed in a heated mold (350°F) and formed to the desired geometry by means of compression provided by fastening the mold.

This foam core is cut into two pieces to provide cores for D spar and trailing edge separately. First, a composite D spar is built using matched-die molding technique. For this, the desired number of composite prepreg layers are laid onto the foam core and each layer is compacted by means of a vacuum pump. The lay-up with foam is placed in the mold, and the assembly is kept in an oven for curing. Thus, a D spar is fabricated. To make a two-cell blade, the cured spar and trailing edge are wrapped by $[+\theta/-\theta]$ layers as skin, and vacuum compacted. This lay-up is kept in the mold and cured in the oven.

Several graphite-epoxy rotor blades of 711.2 mm (28 in.) length, 76.2 mm (3 in.) width, and 9.144 mm (0.36 in.) thickness were fabricated in this manner. These were tested for their structural response under tip bending and torsional loads using a simple test setup.[10] The structural response in terms of bending slope and twist was measured by using a laser optics

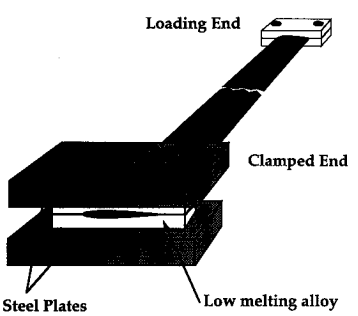

Fig. 4 Details of clamped end of rotor blade.

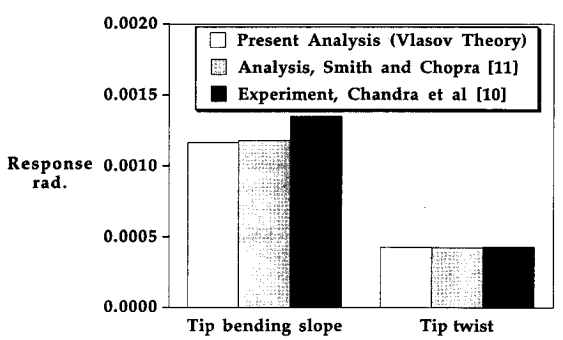

Fig. 5 Response of graphite-epoxy $[0/90]_3$ box beam of slenderness ratio 29 under 1-lb (4.45-N) tip bending and 1-in.-lb (113-N-mm) torsional loads.

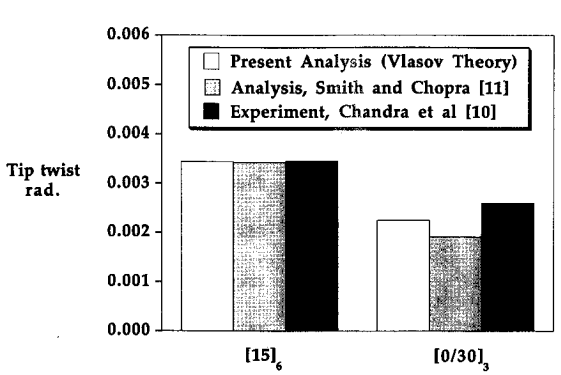

Fig. 6 Tip twist of extension-torsion coupled graphite-epoxy box beams of slenderness ratio 56 under 1-in.-lb (113-N-mm) tip torsional load.

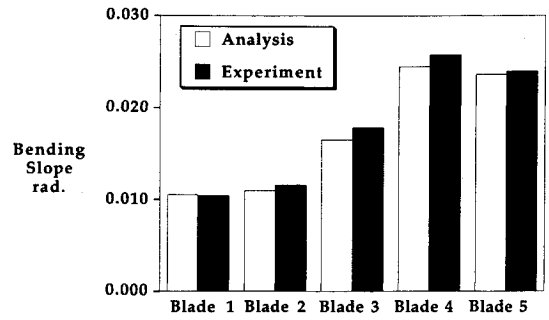

Fig. 7 Influence of lay-up on bending slope of extension-torsion coupled blades of slenderness ratio 72 under 1-lb (4.45-N) tip bending load.

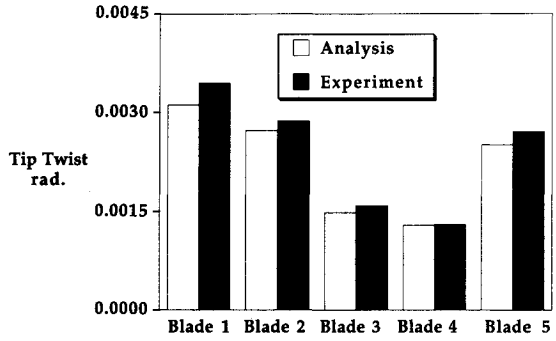

Fig. 8 Influence of lay-up on twist of extension-torsion coupled blades of slenderness ratio 72 under 1-in.-lb (113-N-mm) tip torsional load.

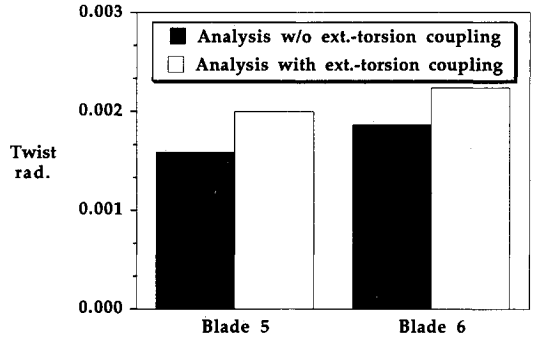

Fig. 9 Influence of extension-torsion coupling on tip twist of extension-torsion coupled blade under 1-in.-lb (113-N-mm) torsional load.

system. Table 1 gives the details of the blades that were fabricated and tested. Figure 4 shows the details of clamped and loading ends of the blade. To simulate the clamped condition accurately, the clamped end was reinforced with additional composite layers.

Results and Discussion

The present analysis is evaluated first for single-cell composite box beams and then validation studies are carried out for two-cell composite blades.

Single-Cell Box Beams

Figure 5 shows the static structural response of thin-walled, graphite-epoxy box beams under 1-lb (4.45-N) tip bending and 1-in.-lb (113-N-mm) tip torsional loads. Note that this beam consists of cross-ply lay-up and, hence, has no bending-torsion coupling. Predicted values are correlated with measured values reported in Ref. 10 and the calculated values of Ref. 11. Present analysis predicts the tip bending slope and twist accurately. Figure 6 shows the tip twist of graphite-epoxy $[15]_6$ and $[0/30]_3$ box beams under 1-in.-lb (113-N-mm) tip torsional load. These beams have antisymmetry with respect to their midaxes and result in extension-torsion and bending-shear couplings. The results of the present analysis correlate better with experimental data for $[0/30]_3$ beams. Thus, the performance of the present analysis in predicting the static structural response of single-cell graphite-epoxy box beams under bending and torsional loads is very good.

Two-Cell Blades with Extension-Torsion Couplings

Structural response of extension-torsion coupled blades under extensional, bending, and torsional loads depends on the geometric and material parameters of the blade, boundary conditions, and loadings. The important blade parameters are ply lay-up and slenderness ratio. Keeping these parameters in view, a parametric study is presented in this paper. To investigate the influence of these parameters on extension-torsion coupling, different blade configurations were examined. The extension-torsion coupling will be significant for blades with all angle plies; however, these blades will have excessive twist induced by curing temperatures. This curing temperature induced twist may be alleviated by introducing 0-deg layers between the angle plies. Also, the hygrothermally stable lay-up eliminates this induced twist. Table 1 shows the details of the blade lay-ups.

Figure 7 shows the tip bending slope of several blades under 1-lb (4.45-N) tip bending load. The correlation between analysis and experiment is within 7%. This figure also indicates the influence of lay-up of blades on bending flexibility. Note the existence of maximum bending flexibility for the blade with 45-deg fiber orientation. Figure 8 illustrates the tip twist of these blades under 1-in.-lb (113-N-mm) tip torsional load. Again, the correlation between analysis and experiment is within 7%. It is to be noted that minimum torsional flexibility occurs for the blade with 45-deg fiber orientation.

Figure 9 shows the influence of extension-torsion coupling on tip twist of extension-torsion coupled blades subjected to 1-in.-lb (113-N-mm) tip torsional load. For these configurations, extension-torsion coupling increases tip twist by about 25%. Figure 10 shows the influence of bending-shear coupling

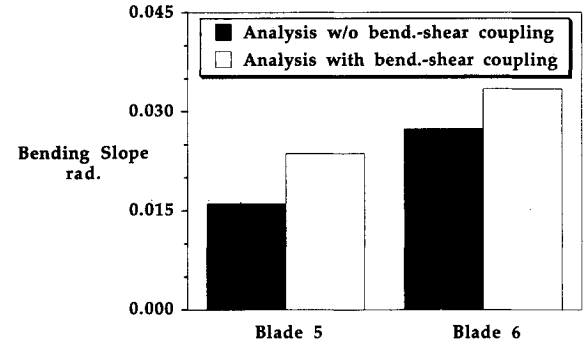

Fig. 10 Influence of bending-shear coupling on tip bending slope of extension-torsion coupled blades under 1-lb (4.45-N) tip bending load.

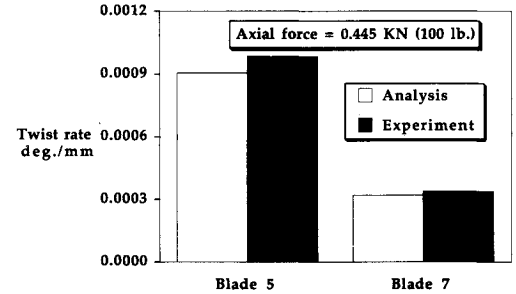

Fig. 11 Twist rates of extension-torsion coupled rotor blades under axial force.

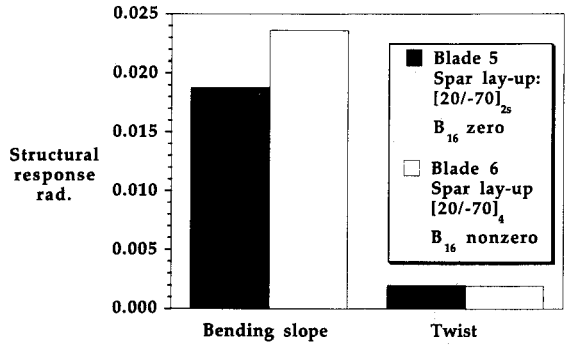

Fig. 12 Influence of B_{16} of spar plate segment of extension-torsion coupled rotor blade under 1-lb (4.45-N) bending and 1-in.-lb (113-N-mm) torsional loads on its structural response.

on bending slope of extension-torsion coupled blades subjected to 1-lb (4.45-N) tip bending load. For the blade with hygrothermally stable lay-up, bending shear coupling increases bending slope by about 50%.

Figure 11 shows the twist rates for two blade configurations (blades 5 and 7). Good correlation between theory and experiment is achieved. The hygrothermally stable lay-up [20, −70] (Ref. 22) provides the induced twist rate of 0.001 deg/mm (0.025 deg/in.) at axial force of 0.445 kN (100 lb). This value may be sufficient in satisfying the requirement for the design of extension-twist coupled tilt rotor blades JVX and XV-15 rotors.[20] To assess the load carrying capability of this blade under extensional load, the strain levels in its different branches were computed. The maximum strains were of the order of 800 microstrains at an axial load of 4.45 kN (1000 lb); these values are well within the material allowables of the blade. Hence, this implies that the blade may be able to resist a 4.45-kN (1000-lb) axial load. Note that the induced twist rate of this blade at 4.45 kN (1000 lb) would be of the order of 0.01 deg/mm (0.25 deg/in.)

Figure 12 shows the influence of extension-twist coupling stiffness B_{16} of the general plate segment of the blade on its structural response under tip bending and torsional loads. The general plate segment of the spar of blade 5 is symmetric with respect to its own midplane, and, hence, B_{16} equals zero. Whereas the spar of blade 6 is made of laminates that are unsymmetric with respect to their midplane and, hence, B_{16} is nonzero. B_{16} influences the bending slope of the blade by increasing the bending-transverse shear coupling K_{26}. About a 25% increase in the bending slope due to B_{16} is noticed for this blade. Note that the twist is virtually unaffected by B_{16}. This is because the torsional stiffness of the blade does not depend on B_{16}. This effect will not be captured by the analysis, where bending stiffness of the wall of the blade is not included.[15]

Conclusions

Two-cell rotor blades made out of general composite laminates were analyzed using Vlasov theory. Transverse shear deformation of the cross section of the blade was included in the analysis. To provide the experimental correlation to the analysis, graphite-epoxy rotor blades with D spar and skin were fabricated using a matched-die molding technique. These blades were tested for elastic response under bending and torsion loads. Good correlation between analysis and experiment was achieved. Based on this study, the following conclusions are made.

1) The influence of bending-transverse shear and extension-torsion coupling on the structural behavior of coupled blades depends on the lay-up. For the blade with hygrothermally stable lay-up, the bending-transverse shear coupling increases the bending flexibility by about 50%.

2) The branches of a generally coupled composite rotor blade must be modeled as general composite laminates. B_{16} of a general plate segment of a blade with hygrothermally stable lay-up increases its bending slope by increasing the bending-transverse shear coupling by about 25%.

3) The induced twist rate of the order of 0.01 deg/mm (0.25 deg/in.) length in a blade with hygrothermally stable configuration can be achieved by an axial load of 4.45 kN (1000 lb). Such coupled blades can be exploited for tilt-rotor design.

Appendix: Relevant Coefficients of Stiffness Matrix [K] of Extension-Torsion Coupled Blades

$$A_{ij} = \sum_{k=1}^{\#\text{ of layers}} Q_{ij}^{(k)}(h_{k+1} - h_k) \tag{A1}$$

$$B_{ij} = \frac{1}{2}\sum_{k=1}^{\#\text{ of layers}} Q_{ij}^{(k)}(h_{k+1}^2 - h_k^2) \tag{A2}$$

$$D_{ij} = \frac{1}{3}\sum_{k=1}^{\#\text{ of layers}} Q_{ij}^{(k)}(h_{k+1}^3 - h_k^3) \tag{A3}$$

where $Q_{ij}^{(k)}$ refers to stiffness matrix of the kth layer in sz plane; h_{k+1} and h_k are coordinates of the kth layer in the n direction from midplane of laminates as reference surface.

$$K_{11} = \int_s A_{11}\, ds \tag{A4}$$

$$K_{15} = \int_s \left[-2B_{16} + \frac{A_{16}}{A_{66}} G_s \right] ds \tag{A5}$$

$$K_{22} = \int_s [A_{11}y^2 + 2B_{11}y\cos\theta + D_{11}\cos^2\theta]\, ds \tag{A6}$$

$$K_{26} = \int_s [A_{16}y\cos\theta + B_{16}\cos^2\theta]\, ds \tag{A7}$$

$$K_{33} = \int_s [A_{11}x^2 + 2B_{11}x\sin\theta + D_{11}\sin^2\theta]\, ds \tag{A8}$$

$$K_{37} = \int_s [A_{16}x\sin\theta + B_{16}\sin^2\theta]\, ds \tag{A9}$$

$$K_{44} = \int_s [D_{11}q^2 + 2B_{11}q\varphi + A_{11}\varphi^2]\, ds \tag{A10}$$

$$K_{55} = \int_s \left[4D_{66} + \frac{G_s^2}{A_{66}} - 4\frac{B_{66}G_s}{A_{66}} \right] ds \tag{A11}$$

$$K_{66} = \int_s A_{66}\cos^2\theta\, ds \tag{A12}$$

$$K_{77} = \int_s A_{66}\sin^2\theta\, ds \tag{A13}$$

Acknowledgments

This research work was supported by the Army Research Office under Contract DAAL-03-88-C-022, Technical Monitors, Robert Singleton and Tom Doligalski.

References

[1]Johnson, A. F., "Bending and Torsion of Anisotropic Beams," *International Journal of Solids and Structures*, Vol. 9, 1973, pp. 527-551.

[2]Minguet, P., and Dugundji, J., "Experiments and Analysis for Composite Blades under Large Deflections Part 1: Static Behavior," *AIAA Journal*, Vol. 28 , No. 9, 1990, pp. 1573-1579.

[3]Minguet, P., and Dugundji, J., "Experiments and Analysis for Composite Blades under Large Deflections Part 2: Dynamic Behavior," *AIAA Journal*, Vol. 28 , No. 9, 1990, pp. 1580-1588.

[4]Chandra, R., and Chopra, I., "Experimental and Theoretical Analysis of Composite I-beams with Elastic Couplings," *AIAA Journal*, Vol. 29, No. 12, 1991, pp. 2197-2206.

[5]Chandra, R., and Chopra, I., "Vibration Characteristics of Composite I-Beams with Elastic Couplings Under Rotation," *Proceedings*

of the 47th Annual Forum of American Helicopter Society, (Phoenix, AZ), May 1991; *Journal of Aircraft* (to be published).

[6]Vlasov, V. Z., "Thin-Walled Elastic Beams," Translated from Russian, National Science Foundation and Department of Commerce, USA, 1961.

[7]Gjelsvik, A., *The Theory of Thin-Walled Bars,* Wiley, New York, 1981.

[8]Rehfield, L. W., and Atilgan, A. R., "On the Buckling Behavior of Thin Walled Laminated Composite Open Section Beams," *Proceedings of the 30th AIAA/ASME/ASCE/AHS/ASC Structures, Structural Dynamics and Materials Conference,* AIAA, Washington, DC, April 1989.

[9]Hong, C. H., and Chopra, I., "Aeroelastic Stability of a Composite Blade," *Journal of the American Helicopter Society,* Vol. 30, No. 2, April 1985, pp. 57–67.

[10]Chandra, R., Stemple, A. D., and Chopra, I., "Thin-Walled Composite Beams under Bending, Torsional and Extensional Loads," *Journal of Aircraft,* Vol. 27, No. 7, 1990, pp. 619–627.

[11]Smith, E. C., and Chopra, I., "Formulation and Evaluation of an Analytical Model for Composite Box Beams," *Journal of the American Helicopter Society,* Vol. 36, No. 3, July 1991, pp. 23–35.

[12]Chandra, R., and Chopra, I., "Experimental-Theoretical Investigation of the Vibration Characteristics of Rotating Composite Box Beams," *Journal of Aircraft,* Vol. 29, No. 4, 1992, pp. 657–664.

[13]Rehfield, L. W., Atilgan, A. R., and Hodges, D. H., "Nonclassical Behavior of Thin-Walled Composite Beams with Closed Cross-Sections," *Journal of the American Helicopter Society,* Vol. 35, No. 2, May 1990, pp. 42–51.

[14]Hodges, D. H., Atilgan, A. R., Fulton, M. V., and Rehfield, L. W., "Free-vibration Analysis of Composite Beams," *Journal of the American Helicopter Society,* Vol. 36, No. 3, July 1991, pp. 36–47.

[15]Rehfield, L. W., Atilgan, A. R., and Hodges, D. H., "Structural Modeling for Multicell Composite Rotor Blades," *Proceedings of the 28th AIAA/ASME/ASCE/AHS/ASC Structures, Structural Dynamics and Materials Conference,* AIAA, Washington, DC, April 1988.

[16]Kosmatka, J. B., "Extension-Bend-Twist Coupling Behavior of Thin-walled Advanced Composite Beams with Initial Twist," *Proceedings of the 32nd AIAA/ASME/ASCE/AHS/ASC Structures, Structural Dynamics and Materials Conference,* AIAA, Washington, DC, April 1991.

[17]Bauchau, O. A., and Hong, C. H., "Large Displacement Analysis of Naturally Curved and Twisted Composite Beams," *AIAA Journal,* Vol. 25, No. 11, 1987, pp. 1469–1475.

[18]Giavotto, V., Borri, M., Mantegazza, P., Ghiringhelli, G., Carmaschi, V., Maffioli, G. C., and Mussi, F., "Anisotropic Beam Theory and Applications," *Computers and Structures,* Vol. 16, Nos. 1–4, 1983, pp. 403–413.

[19]Borri, M., and Merlini, T., "A Large Displacement Formulation for Anisotropic Beam Analysis," *Meccanica,* Vol. 21, 1986, pp. 30–37.

[20]Nixon, M. W., "Extension-Twist Coupling of Composite Circular Tubes with Application to Tilt Rotor Blade Design," *Proceedings of the 28th AIAA/ASME/ ASCE/AHS/ASC Structures, Structural Dynamics and Materials Conference,* AIAA, Washington, DC, April 1987.

[21]Chandra, R., and Chopra, I., "Structural Behavior of Two-Cell Composite Rotor Blades With Elastic Couplings," *Proceedings of the Seventeenth European Rotorcraft Forum,* (Berlin, Germany), Sept. 1991.

[22]Winckler, S. J., "Hygrothermally Curvature Stable Laminates with Tension-Torsion Coupling," *Journal of the American Helicopter Society,* Vol. 30, No. 3, July 1985, pp. 56–58.